Calculation of the photodetachment cross sections of the HCN^- and HNC^- dipole-bound anions as described by a one-electron Drude model

M. Sindelka,[a] V. Spirko, and P. Jungwirth
Institute of Organic Chemistry and Biochemistry, Academy of Sciences of the Czech Republic, and Center for Complex Molecular Systems and Biomolecules, Flemingovo nam. 2, 16610 Prague 6, Czech Republic

F. Wang,[b] S. Mahalakshmi,[c] and K. D. Jordan
Department of Chemistry and Center for Molecular and Materials Simulations, University of Pittsburgh, Pittsburgh, Pennsylvania 15260

(Received 1 March 2004; accepted 6 May 2004)

The Drude model for treating the interaction of excess electrons with polar molecules is extended to calculate continuum functions and to evaluate photodetachment cross sections. The approach is applied to calculate the cross sections for photodetachment of dipole-bound electrons from HCN^- and HNC^-. In addition, an adiabatic model separating the angular and radial degrees of freedom of the excess electron is introduced and shown to account in a qualitative manner for the cross sections.
 [DOI: 10.1063/1.1766296]

I. INTRODUCTION

The problem of the interaction of excess electrons with polar molecules has a long and fascinating history. Within the context of the Born-Oppenheimer (BO) approximation, there is a critical dipole moment of 1.625 D for binding an excess electron in a dipole field, giving a so-called dipole-bound anion.[1–4] When corrections to the BO approximation are included, the critical moment becomes dependent on the moments of inertia, but as a rule of thumb it is increased to about 2.4 D.[5,6] For molecules with dipole moments appreciably greater than this, corrections to the BO approximation cease to be important (at least for the ground electronic state).

The orbital occupied by the excess electron in a dipole-bound anion has very little charge density in the molecular region. As a result, it was long believed that electron correlation effects do not play an important role in the excess electron binding. However, in recent years it has been shown that dispersion interactions between the excess electron and the electrons of the polar molecule are important, causing, in general, a large increase in the magnitude of the electron binding energy and contraction of the wave function.[7–10] To accurately describe the binding energy of the excess electron using traditional *ab initio* electronic structure methods requires the use of large, flexible basis sets and inclusion of electron correlation effects to high order.[7–11]

To date, most of the theoretical investigations of dipole-bound anions have focused on the calculation of the binding energies. Surprisingly little theoretical work has been done on the photodetachment cross sections even though they are accessible experimentally. Calculations of photodetachment cross sections of dipole-bound anions are especially challenging given the need to accurately characterize both the bound state and continuum wave functions.

Recently, Wang and Jordan introduced a Drude model approach permitting the dispersion interactions between the excess electron and the neutral polar molecule to be recovered within a one-electron framework and showed that this approach accurately describes the binding of the excess electron in dipole-bound anions.[9–11] In the present study we extend the Drude model to the calculation of the continuum wave functions and photodetachment cross sections of dipole-bound electrons, applying the formalism to HCN^- and HNC^-.

II. THEORETICAL BACKGROUND

A. Bound and continuum states of the excess electron

The starting point for the present study is the assumption that the molecular dipole moments are sufficiently large so that corrections to the BO approximation can be ignored. This should be a good approximation for HCN^- and HNC^-, for which the rotational energies are appreciably smaller than the BO electron binding energies. (Large basis set CCSDT calculations give electron binding energies of -13.2 and $-36.7\ cm^{-1}$, for HCN^- and HNC^-, respectively.[12]) The total Hamiltonian (in atomic units) can be written as

$$H = H_e + H_{DO} + H_{couple}, \tag{1}$$

where the individual terms are defined as

$$H_e = -\tfrac{1}{2}\nabla_r^2 + V(\mathbf{r}), \tag{2}$$

[a]Present address: Department of Chemistry, Technion—Israel Institute of Technology, Haifa 32000, Israel.
[b]Present address: Department of Chemistry, University of Utah, Salt Lake City, Utah 84112.
[c]Present address: Indian Institute of Technology Madras, Chennai—60036, India.

TABLE I. Dipole moments and electron binding energies (E_b) of HCN and HNC.[a]

	Dipole moment		E_b (cm^{-1})			
					Drude	
Molecule	Method	Value (a.u.)	Method	*Ab initio*[b]	3D	*r*-adiab.
HCN	HF	1.308	KT	−11.60	−11.60	−11.97
	CCSD(T)	1.204	CI/CCSDT	−13.21	−13.21	−15.91
HNC	HF	1.127	KT	−3.22	−3.22	−3.37
	CCSD(T)	1.213	CI/CCSDT	−35.68	−35.68	−49.14

[a]The charges used for the KT and CI calculations within the context of the Drude model, reproduce, respectively, the dipole moments from *ab initio* Hartree-Fock (HF) and CCSD(T) calculations.
[b]The KT and CCSDT *ab initio* electron binding energies from Ref. 12 were obtained from calculations using large Gaussian orbital basis sets.

$$H_{\mathrm{DO}} = -\frac{1}{2m_o}\nabla_R^2 + \frac{1}{2}k_\perp(X^2+Y^2) + \frac{1}{2}k_\parallel Z^2, \tag{3}$$

and

$$H_{\mathrm{couple}} = \frac{q\mathbf{r}\cdot\mathbf{R}}{r^3}(1-e^{-br^2}). \tag{4}$$

r denotes the vector position of the excess electron, and **R** is associated with the Drude oscillator, described below. The electronic Hamiltonian H_e describes the motion of an excess electron in the field of the pseudopotential $V(\mathbf{r})$, H_{DO} is the Hamiltonian for the Drude oscillator, and H_{couple} describes the coupling of the excess electron and the Drude oscillator. $V(r)$ includes the electrostatic interactions between the excess electron and point charges used to represent the charge distribution of the molecule as well as a term to represent the repulsion between the excess electron and the electrons of the neutral molecule. The Drude oscillator consists of point charges $+q$ and $-q$ coupled harmonically with the force constants $k_\parallel$ and $k_\perp$. The $+q$ charge is taken as fixed, while the $-q$ charge is mobile, the location of which is given by **R**. $q^2/k_\parallel$ and $q^2/k_\perp$ are chosen so as to reproduce the experimental values of the anisotropic polarizability ($\alpha_\parallel$ and $\alpha_\perp$, respectively) of the neutral HCN or HNC molecule. The mass m_o associated with the Drude oscillator is taken to be the electron mass. The $(1-e^{-br^2})$ factor in H_{couple} damps out the nonphysical short-range interaction.

The eigenvalue equation for the isolated Drude oscillator is

$$H_{\mathrm{DO}}\Xi_v(\mathbf{R}) = \epsilon_v^{\mathrm{DO}}\Xi_v(\mathbf{R}). \tag{5}$$

Due to the use of an anisotropic polarizability, Ξ_v is represented as a product of *X*-, *Y*-, and *Z*-dependent harmonic oscillator functions, and v stands for the collection of quantum numbers, v_X, v_Y, and v_Z. The excitation energies of the Drude oscillator, $(\epsilon_v^{\mathrm{DO}}-\epsilon_o^{\mathrm{DO}})$, are comparable to the electronic excitation energies of the neutral molecule.

Stationary states of the model system with *H* given by Eq. (1) are obtained by solving the Schrödinger equation,

$$H\psi(\mathbf{r},\mathbf{R}) = E\psi(\mathbf{r},\mathbf{R}). \tag{6}$$

Equation (6) admits an infinity of bound states for molecules with dipole moments $\mu > 1.625$ D. However, given the small ($\approx$3.1 D) dipole moments of HCN and HNC, only the lowest of these would persist were corrections to the BO approximation included.[5,6] The continuum wave functions are constructed so as to satisfy the generalized orthogonality relations

$$\langle\psi_{E\xi}|\psi_{E'\xi'}\rangle = \delta(E-E')\,\delta_{\xi,\xi'}, \tag{7}$$

where ξ is an index used to distinguish the various linearly independent continuum functions of energy *E*.[13]

B. Photodetachment cross section

For weak field intensities, the expression for the photodetachment cross section takes the form

$$\sigma(E) = \frac{4\pi^2}{3}\frac{\beta}{e^2}(E-E_b)\sum_\xi |\langle\psi_{E\xi}|\mathbf{d}|\psi_b\rangle|^2, \tag{8}$$

where the transition moment operator $\mathbf{d}(\mathbf{r},\mathbf{R})$ depends on the coordinates of both the excess electron and the Drude oscillator, β is the dimensionless fine structure constant, $\psi_{E\xi}$ is a wave function associated with a continuum state, and ψ_b and E_b are, respectively, the wave function and energy associated with the most stable bound state of the excess electron.[14,15] Integration in Eq. (8) is over both **r** and **R**.

C. Pseudopotentials

Table I reports the dipole moments and electron binding energies obtained from *ab initio* calculations. Whereas inclusion of electron correlation effects causes about a 0.1 D decrease in the dipole moment of HCN, it causes a 0.1 D increase in the dipole moment of HNC. These relatively small dipole moment changes are accompanied by large changes in the electron binding energies,[9] making it essential that the model potentials accurately describe the dipole moments of the molecules of interest.

Two different sets of calculations were performed for each dipole-bound anion. The first is in the spirit of the Koopmans' theorem (KT) approximation[16] and neglects the coupling of the excess electron with the Drude oscillator, while the second adopts a configuration interaction (CI) approach to calculate the energy of the electron-Drude oscillator system. The CI calculations allow for correlation effects via inclusion of configurations involving simultaneous excitation of the dipole-bound electron and the Drude oscillator.

The methodology for calculating the energies within the framework of the pseudopotential model is given in Sec. III A. The pseudopotentials were adopted from Ref. 9. Here we note that the electrostatic part of the pseudopotential was represented by three atom-centered point charges. For the KT calculations these were chosen so as to reproduce the *ab initio* Hartree-Fock dipole moment, and for the CI calculations the charges were chosen so as to reproduce the *ab initio* CCSD(T) dipole moment (see Table I) of the molecule of interest.

The repulsive potentials used in the pseudopotential calculations were chosen so that the resulting electron binding energies calculated using the KT-like procedure reproduced the *ab initio* KT values. In addition, the parameter b in the damping factor in the coupling term was chosen for each system so that the binding energy from the CI-level model potential calculations reproduces the *ab initio* CCSDT result (see Table I).[12]

III. COMPUTATIONAL METHODOLOGY

A. Close-coupling approach

Numerical solution of the Schrödinger equation (5) is based on a wave function expansion employing products of electronic and Drude oscillator functions:

$$\psi(\mathbf{r},\mathbf{R})=\frac{1}{r}\sum_{s,v}F_{sv}(r)Y_s(\theta,\phi)\Xi_v(\mathbf{R}), \tag{9}$$

where $F_{sv}(r)$ and $Y_s(\theta,\varphi)$ are, respectively, the radial functions and spherical harmonics used to describe the excess electron, and the $\Xi_v(\mathbf{R})$ are eigenfunctions associated with the Drude oscillator. s is a collective index for both the l_s and m_s quantum numbers. For the KT-like calculations only the lowest energy Drude oscillator function Ξ_o is retained, so that the excess electron and the Drude oscillator are uncorrelated. In the CI treatment, the lowest excited states in each of the X, Y, and Z degrees of freedom are also included for the Drude oscillator. Using the expansion in Eq. (9), the eigenvalue problem is transformed to a system of coupled second-order differential equations for the radial functions

$$-\frac{1}{2}\frac{d^2}{dr^2}F_{sv}(r)+\sum_{s'v'}W_{sv}^{s'v'}(r)F_{s'v'}(r)=EF_{sv}(r), \tag{10}$$

where

$$\begin{aligned}W_{sv}^{s'v'}(r)=&\delta_{ss'}\delta_{vv'}\left[\frac{l_s(l_s+1)}{2r^2}+\epsilon_v^{\mathrm{DO}}\right]+\delta_{vv'}\\&\times\int_0^{2\pi}d\phi\int_0^{\pi}\sin\theta\,d\theta[Y_s^*(\theta,\phi)V(r)Y_{s'}(\theta_s\phi)]\\&+\int_0^{2\pi}d\phi\int_0^{\pi}\sin\theta\,d\theta\int d\mathbf{R}[Y_s(\theta,\phi)\Xi_v^*(\mathbf{R})\\&\times H_{\mathrm{couple}}(\mathbf{r},\mathbf{R})Y_{s'}(\theta,\phi)\Xi_{v'}(\mathbf{R})].\end{aligned} \tag{11}$$

For the bound states the system of equations is solved subject to the boundary conditions that $F\to 0$ in the $r\to 0$ and $r\to\infty$ limits. For the continuum states $F\to 0$ in the $r\to 0$ limit, whereas the procedure described in Ref. 13 is used to deal with the boundary condition on F in the $r\to\infty$ limit.

The matrix elements contributing to the photodetachment cross section may be expressed as

$$\langle\psi_b|\mathbf{d}|\psi_{E\xi}\rangle=\sum_{s_1,v_1}\sum_{s_2,v_2}\int_0^{\infty}F_{s_1v_1}^{r}D_{s_1v_1}^{s_2v_2}(r)F_{s_2v_2}^{E,\xi}dr \tag{12}$$

with

$$\begin{aligned}D_{s_1v_1}^{s_2v_2}(r)=&\int_0^{2\pi}d\phi\int_0^{\pi}\sin\theta\,d\theta\int d\mathbf{R}\\&\times[Y_{s_1}^*(\theta,\phi)\Xi_{v_1}^*(R)\mathbf{d}(\mathbf{r},\mathbf{R})Y_{s_2}(\theta,\phi)\Xi_{v_2}(\mathbf{R})].\end{aligned} \tag{13}$$

B. The *r*-adiabatic treatment

In addition to the numerically exact solution of the Schrödinger equation (5), we also considered a one-dimensional adiabatic model separating r from the remaining ($\mathbf{R}$, θ, and φ) degrees of freedom. This model was derived by first ignoring the differential operator $(-1/2)(d^2/dr^2)$ in Eq. (10), and by diagonalizing the Hermitian matrix W by use of a unitary transformation

$$U^{+}(r)W(r)U(r)=\mathrm{diag}\{w_{sv}(r)\} \tag{14}$$

to obtain a set of effective r-adiabatic potentials $w_{sv}(r)$. As a second step this transformation was applied to the original coupled channel problem (10), neglecting all nonadiabatic coupling terms arising from the noncommutation of the operators U and (d^2/dr^2). This procedure leads to a system of uncoupled one-dimensional radial equations

$$\left[-\frac{1}{2}\frac{d^2}{dr^2}+w_{sv}(r)\right]F_{sv}(r)=EF_{sv}(r). \tag{15}$$

The overall wave functions are

$$\psi^{sv}(\mathbf{r},\mathbf{R})=(1/r)F_{sv}(r)\Psi_{sv}(r,\theta,\phi,\mathbf{R}), \tag{16}$$

with the adiabatic basis functions

$$\Psi_{sv}(r,\theta,\phi,\mathbf{R})=\sum_{s'v'}U_{sv}^{s'v'}(r)Y_{s'}(\theta,\phi)\Xi_{v'}(\mathbf{R}) \tag{17}$$

being only parametrically dependent on the radial variable r. It is not obvious *a priori* how useful the adiabatic model will be for an excess electron bound in a dipole field. As will be demonstrated below, this approximation works surprisingly well.

C. Expansion in spherical harmonics and grids

Our test calculations indicated that convergence of the excess electron binding energies of the HCN^- and HNC^- species was achieved for $l_{\max}=5$ and $|m|_{\max}=1$. The truncated system of coupled equations was solved numerically on an equidistant radial grid, using the renormalized Numerov method of Johnson.[17] The increment of the radial grid was taken to be 0.05 bohr, and integration was carried out from zero to $r_{\max}$ ranging from 500 to 2000 bohr, depending on the degree of delocalization of the bound state wave func-

tion. The matrix elements [Eqs. (11) and (13)] were simplified by analytical integration over R. The remaining two-dimensional (2D) integration was carried out numerically via a Gauss-Legendre quadrature scheme, using about 50 mesh points for the θ variable and 100 mesh points for the φ variable. The one-dimensional integrals from Eq. (12) were evaluated by summations over the radial grid points.

IV. RESULTS AND DISCUSSION

A. Bound states of the excess electron

By design, the model potentials, solved using the full 3D close coupling approach, give nearly the same electron binding energies at both the KT and CI levels of theory as obtained from the corresponding *ab initio* calculations (here, the Drude model CI results are compared with *ab initio* CCSDT results). For both HCN and HNC, inclusion of electron correlation effects in the *ab initio* calculations causes an increase in the magnitude of the electron binding energy, with the increase being only 14% for HCN but over tenfold for HNC. To a large extent, the different behavior of these two molecules can be understood in terms of the changes in the dipole moments upon inclusion of correlation effects as was discussed in Ref. 9. Specifically, inclusion of electron correlation effects in the *ab initio* calculations leads to an increase in the dipole moment of HNC and a decrease in the dipole moment of HCN, which, in turn, causes enhanced binding of the excess electron to HNC and weakened binding of the excess electron to HCN. However, as mentioned in the Introduction, there is also a dispersion-type interaction between the excess electron and the electrons of the neutral molecule, which necessarily acts so as to increase the binding of the excess electron. Thus the large enhancement of the binding of the excess electron to HNC upon inclusion of electron correlation is a consequence of the two effects reinforcing one another, and the relatively small enhancement in the case of HCN is due to their operating in different directions (i.e., with the dipole change acting so as to weaken the binding and the dispersion interactions acting so as to enhance it). In the Drude model the impact of electron correlation on the dipole moment of the neutral molecule is incorporated via a ''renormalization'' of the atomic charges.

The electron binding energies obtained from both the full 3D treatment as well as the r-adiabatic approximation to the one-electron Drude model are also included in Table I. The r-adiabatic approximation leads to an overestimation of the magnitude of the electron binding energies, with the overestimation being less than 5% at the KT level and 28%–38% at the CI level. Figure 1 shows radial distributions of the excess electron of HNC^- as described by the one-electron Drude model at both the KT and CI levels of theory, and calculated using the full 3D treatment as well as in the r-adiabatic approximation. As noted in previous studies,[9–11] the inclusion of correlation effects causes a significant contraction of the excess electron wave function. As will be seen below, this, in turn, is responsible for the reduction of the photodetachment cross section. In the KT approximation the wave functions obtained from the r-adiabatic and full 3D treatments are nearly identical. However, incorporation of correlation effects leads to a greater contraction of the wave function in the r-adiabatic than in the full 3D calculations. Nonetheless, the contraction of the wave function brought about by inclusion of correlation effects is far greater than that resulting from use of the r-adiabatic approximation.

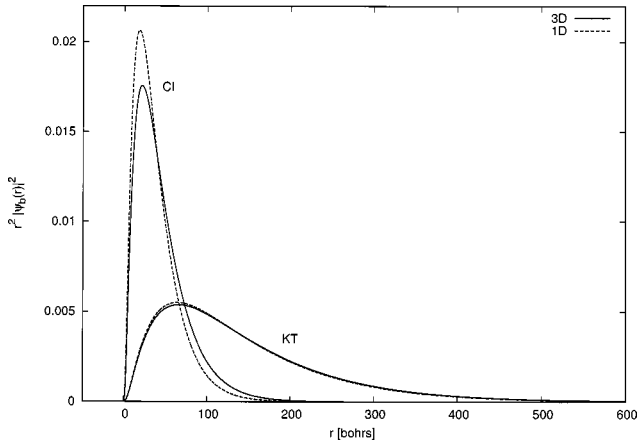

FIG. 1. Radial distribution of an excess electron for HNC^-, calculated at the KT and CI levels of theory using the full three-dimensional treatment (solid curves) as well as with the one-dimensional r-adiabatic model (dashed curves).

B. Photodetachment cross sections

The dipole moment operator **d**, depends on the charges associated with the Drude oscillator as well as on the charge distribution of the excess electron. However, our test calculations reveal that the transition moment integrals for HCN^- and HNC^- are almost entirely determined (i.e., to 99%) by the portion of the dipole operator associated with the excess electron. Thus, while correlation effects between the excess electron and the electrons of the neutral molecule are very important for the shape of the bound state wave function as well as for the near threshold continuum functions, photodetachment is essentially a one-electron process.

Figure 2 depicts the bound and two selected continuum

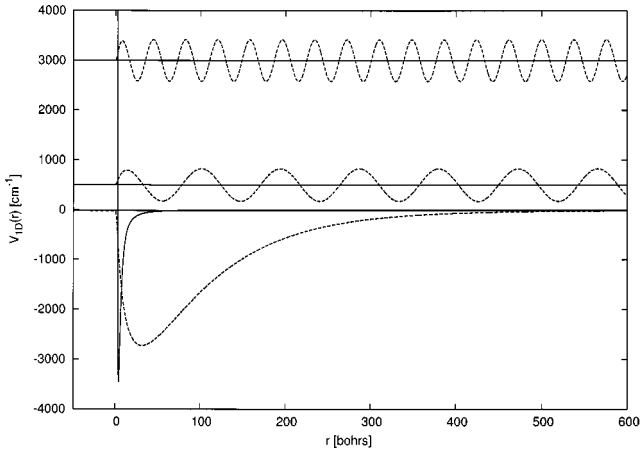

FIG. 2. One-dimensional r-adiabatic eigenstates $F_{10}(r)$ calculated at the CI level of theory for HCN^-. The dashed curves depict the bound and two selected continuum eigensolutions of Eq. (15), corresponding to energy levels of -15.9, 500, and 3000 cm^{-1}, respectively. The solid curve shows the effective potential $w_{10}(r)$ associated with the lowest r-adiabatic channel.

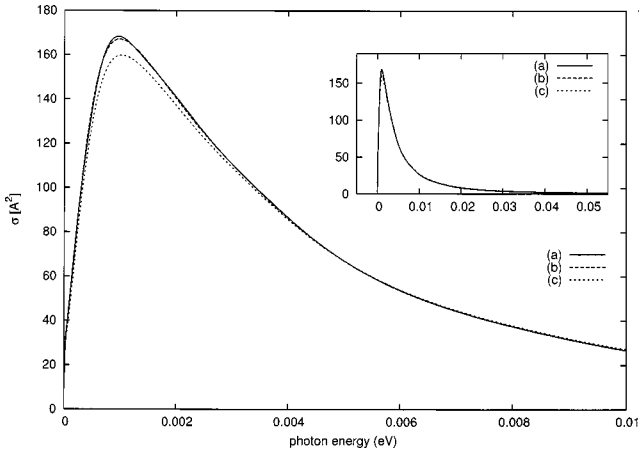

FIG. 3. Photodetachment cross section $\sigma(E)$ for HCN^- calculated at the KT level of theory using the one-electron model described in the text. Profile (a) was obtained using an "exact" three-dimensional treatment of the bound and continuum states of the excess electron. Profile (b) was obtained by treating the continuum states in the *r*-adiabatic approximation, and profile (c) was obtained by treating both the bound and continuum states in the *r*-adiabatic approximation.

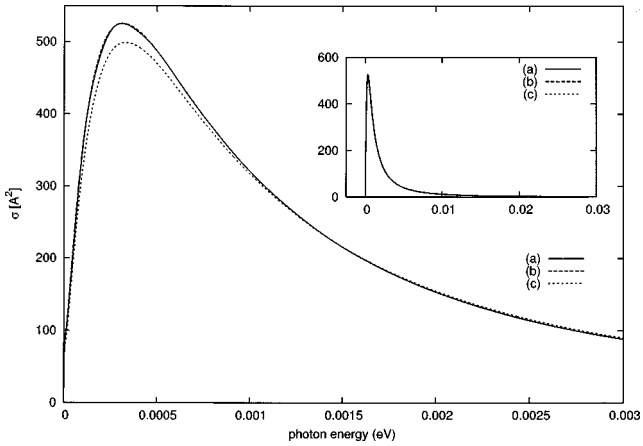

FIG. 5. Photodetachment cross section $\sigma(E)$ for HNC^- calculated at the KT level of theory using the one-electron model described in the text. Profile (a) was obtained using an "exact" three-dimensional treatment of the bound and continuum states of the excess electron. Profile (b) was obtained by treating the continuum states in the *r*-adiabatic approximation, and profile (c) was obtained by treating both the bound and continuum states in the *r*-adiabatic approximation.

eigenstates of Eq. (15), with $s=1$ and $v=0$ (which denote $l=0$, $m_l=0$, $v_X=v_Y=v_Z=0$), parameters appropriate for HCN^- and at the CI level. The bound state is highly delocalized, which is responsible for the large magnitudes of the photodetachment cross sections. The fact that the transition dipole moment operator grows linearly with increasing r makes the long-range tails of the bound-state wave functions especially important for the photodetachment cross sections.

For both anions and for each theoretical approach used, the calculated cross section rises rapidly from threshold and then decays smoothly to zero as $E\to\infty$ (see Figs. 3–6). There are no sharp features, consistent with the absence of resonances over the energy ranges considered. As expected, the absolute magnitudes of the cross sections are strongly influenced by the magnitude of the electron binding energy. Specifically, the cross sections are smaller in the CI than in the KT calculations, consistent with the larger (in magnitude) binding energies and greater localization of the excess electron in the CI calculations.

Comparison of the photodetachment cross sections of HCN^- and HNC^- at the KT and CI levels of theory reveals that to a good approximation the peak values of the cross sections fall off as $|E_b|^{-1}$. This is consistent with the behavior expected from an expression of $\sigma(E)$ derived using the asymptotic forms of the bound and continuum wave functions.

Figures 3–6 display also the cross sections calculated using the one-dimensional *r*-adiabatic approach, with only the continuum treated adiabatically as well as with both the

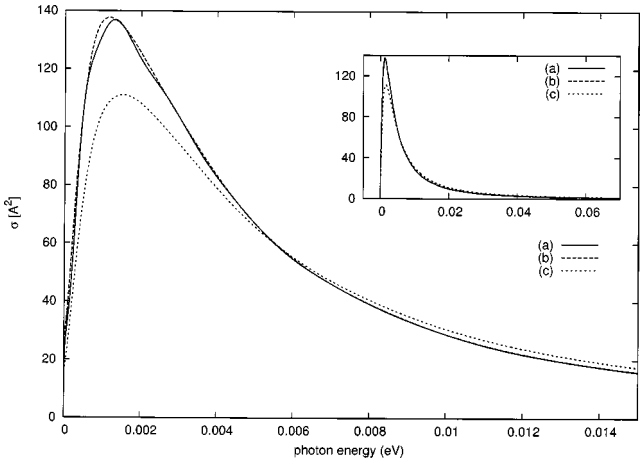

FIG. 4. Photodetachment cross section $\sigma(E)$ for HCN^- calculated at the CI level of theory using the one-electron Drude model described in the text. Profile (a) was obtained using an "exact" three-dimensional treatment of the bound and continuum states of the excess electron. Profile (b) was obtained by treating the continuum states in the *r*-adiabatic approximation, and profile (c) was obtained by treating both the bound and continuum states in the *r*-adiabatic approximation.

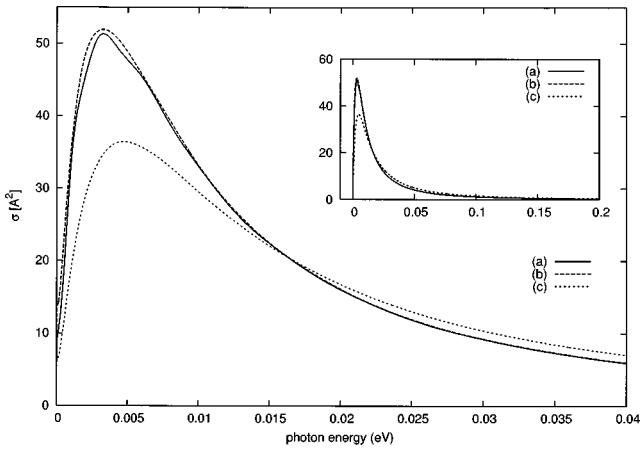

FIG. 6. Photodetachment cross section $\sigma(E)$ for HNC^- calculated at the CI level of theory using the one-electron Drude model described in the text. Profile (a) was obtained using an "exact" three-dimensional treatment of the bound and continuum states of the excess electron. Profile (b) was obtained by treating the continuum states in the *r*-adiabatic approximation, and profile (c) was obtained by treating both the bound and continuum states in the *r*-adiabatic approximation.

continuum and bound state wave functions treated adiabatically. The cross sections calculated with only the continuum functions treated adiabatically are close to those from the full 3D treatment, whereas those calculated using the adiabatic approximation for both the bound and continuum functions differ appreciably from the full 3D results in the calculations carried out at the CI level.

Experimental photodetachment cross sections are not available for HCN^- and HNC^-, so comparison between theory and experiment is not possible for these species. Experimental photodetachment cross sections are available for larger dipole-bound anions including CH_3CN^- and $(H_2O)_6^-$,[18,19] and it is planned to extend our approach to these species.

V. CONCLUSION

The Drude model for treating electron correlation between a weakly bound electron and a polar molecule (or cluster of polar molecules) has been extended to allow for the calculation of continuum eigenfunctions. These were used together with the corresponding bound state wave functions to calculate the photodetachment cross sections of HCN^- and HNC^-. Inclusion of electron correlation effects (recovered via interaction of the excess electron with the Drude oscillator) are found to cause a contraction of the charge distribution of the excess electron, which leads to a sizable reduction in the cross sections. Previous studies have shown that this contraction is due to second and higher-order corrections to the wave function.[9–11] A one-dimensional *r*-adiabatic model is introduced which accounts in a qualitative manner for the electron binding and the photodetachment cross sections.

ACKNOWLEDGMENTS

This research was supported with grants from the National Science Foundation (F.W., M.S., and K.D.J.) and by the Czech Ministry of Education via Grant No. LN00A032 (M.S., V.S., and P.J.). We thank Professor Jack Simons for valuable discussions about the electron-dipole photodetachment problem.

[1] E. Fermi and E. Teller, Phys. Rev. **72**, 399 (1947).
[2] R. E. Wallis, R. Hermans, and H. W. Milnes, J. Mol. Spectrosc. **4**, 51 (1960).
[3] O. H. Crawford, Proc. R. Soc. London **91**, 279 (1967).
[4] J. Simons and K. D. Jordan, Chem. Rev. (Washington, D.C.) **87**, 535 (1987).
[5] W. R. Garrett, Phys. Rev. A **3**, 961 (1971).
[6] O. H. Crawford, Chem. Phys. Lett. **2**, 461 (1968).
[7] M. Gutowski, K. D. Jordan, and P. Skurski, J. Phys. Chem. A **102**, 2624 (1998).
[8] M. Gutowski, P. Skurski, A. I. Boldyrev, J. Simons, and K. D. Jordan, Phys. Rev. A **54**, 1906 (1996).
[9] F. Wang and K. D. Jordan, J. Chem. Phys. **114**, 10717 (2001).
[10] F. Wang and K. D. Jordan, J. Chem. Phys. **116**, 6973 (2002).
[11] K. D. Jordan and F. Wang, Annu. Rev. Phys. Chem. **54**, 367 (2003).
[12] K. A. Peterson and M. Gutowski, J. Chem. Phys. **116**, 3297 (2002).
[13] M. Sindelka, V. Spirko, and P. Jungwirth, J. Chem. Phys. **117**, 5113 (2002).
[14] R. Schinke, *Photodissociation Dynamics* (Cambridge University Press, Cambridge, 1995).
[15] G. G. Balint-Kurti and M. Shapiro, Adv. Chem. Phys. **LX**, 403 (1985).
[16] T. Koopmans, Physica (Amsterdam) **1**, 104 (1934).
[17] B. R. Johnson, J. Chem. Phys. **69**, 4678 (1978).
[18] C. G. Baily, C. E. H. Dessent, M. A. Johnson, and K. H. Bowen, Jr., J. Chem. Phys. **104**, 6976 (1996).
[19] C. G. Baily and M. A. Johnson, Chem. Phys. Lett. **265**, 185 (1997).